

Breaking Complexity Barriers: High-Resolution Image Restoration with Rank Enhanced Linear Attention

Yuang Ai^{1,2} Huaibo Huang^{1,2}✉ Tao Wu^{1,3} Qihang Fan^{1,2} Ran He^{1,2}

¹MAIS & NLPR, Institute of Automation, Chinese Academy of Sciences

²School of Artificial Intelligence, University of Chinese Academy of Sciences

³School of Information Science and Technology, ShanghaiTech University

shallowdream555@gmail.com, huaibo.huang@cripac.ia.ac.cn

Abstract

Transformer-based models have made remarkable progress in image restoration (IR) tasks. However, the quadratic complexity of self-attention in Transformer hinders its applicability to high-resolution images. Existing methods mitigate this issue with sparse or window-based attention, yet inherently limit global context modeling. Linear attention, a variant of softmax attention, demonstrates promise in global context modeling while maintaining linear complexity, offering a potential solution to the above challenge. Despite its efficiency benefits, vanilla linear attention suffers from a significant performance drop in IR, largely due to the low-rank nature of its attention map. To counter this, we propose Rank Enhanced Linear Attention (RELA), a simple yet effective method that enriches feature representations by integrating a lightweight depthwise convolution. Building upon RELA, we propose an efficient and effective image restoration Transformer, named LAformer. LAformer achieves effective global perception by integrating linear attention and channel attention, while also enhancing local fitting capabilities through a convolutional gated feed-forward network. Notably, LAformer eliminates hardware-inefficient operations such as softmax and window shifting, enabling efficient processing of high-resolution images. Extensive experiments across 7 IR tasks and 21 benchmarks demonstrate that LAformer outperforms SOTA methods and offers significant computational advantages.

1. Introduction

Image restoration (IR) aims to recover a high-quality (HQ) image by removing degradations from its degraded low-quality (LQ) counterpart. As a fundamental task in low-level vision, image restoration has a wide array of real-world applications, spanning fields such as autonomous driving [131], surveillance monitoring [78], medical imag-

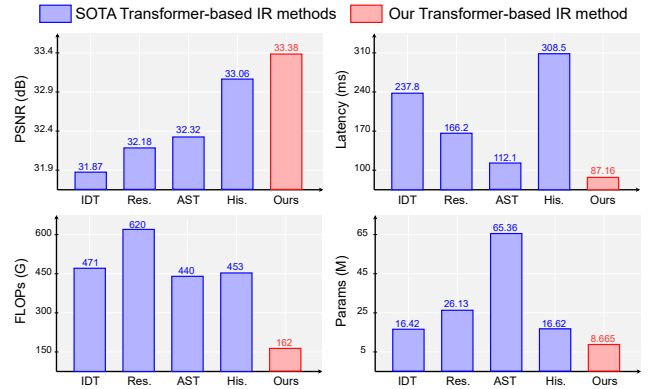


Figure 1. Comparison with Transformer-based methods for rain-drop removal, including IDT [104], Restormer [115], AST [129], and Histoformer [86]. Ours represents LAformer-S. Overhead is evaluated on 512×512 images using a single V100 GPU.

ing [30], etc. Consequently, developing hardware-efficient IR networks holds substantial practical value.

Over the past decade, convolutional neural networks (CNNs) have achieved remarkable progress in various IR tasks [25, 106, 121]. However, CNNs are often limited by their constrained receptive field, making it challenging to capture long-range dependencies. Recently, Transformer-based methods [18, 49, 115] have significantly advanced the performance of image restoration. While Transformer offers the advantage of a global receptive field, its core self-attention mechanism introduces quadratic computational complexity. Directly applying self-attention globally incurs substantial overhead, particularly when handling high-resolution images. To mitigate this, some methods compute self-attention within local windows [17, 50, 98], while others adopt sparse attention patterns [16, 120]. While effectively reducing computational costs, these methods either limit global perception or are sensitive to degradation types due to specific attention patterns [129].

The above analysis leads to a crucial question: *Is it possible to design a hardware-efficient image restoration model*

that simultaneously preserves strong global perceptive capabilities? In this paper, we explore linear attention [36] as a potential solution to this issue. Compared to standard softmax attention [92], linear attention replaces the softmax operation with simpler activation functions (e.g., ReLU [3], ELU [21]) and reorders the computation to first calculate $K^T V$. As shown in Fig. 2, linear attention reduces the computational complexity to a linear scale with respect to the number of visual tokens N , while preserving the global contextual advantages of softmax attention. When processing high-resolution images, the global receptive field of linear attention enables the capture of long-range relationships between pixels, thereby enhancing restoration quality. These attributes motivate us to employ linear attention in developing an efficient and effective image restoration model.

However, standard linear attention mechanisms appear suboptimal for image restoration, resulting in a notable performance drop relative to softmax attention (See Tab. 11). Through rank analysis [49], we find that the low-rank nature of the attention map in linear attention severely limits the diversity of its output features, thereby diminishing its representation capacity (See Fig. 4). To overcome this limitation, we propose Rank Enhanced Linear Attention (RELA), which incorporates a lightweight depthwise convolution to effectively enhance the rank of output feature. RELA retains linear complexity while boosting the representation capacity of linear attention, enabling improved modeling of complex degradation patterns.

We further propose LAformer, an efficient image restoration Transformer structured within the widely adopted U-Net architecture [103, 115]. As shown in Fig. 3, LAformer incorporates a Dual-Attention (DA) Block that operates across spatial and channel dimensions, leveraging both RELA and channel attention [124] concurrently to facilitate efficient global information capture. Recognizing the crucial role of local information in restoring texture details, we introduce a Convolutional Gated Feed-Forward Network (CG-FFN) to strengthen LAformer’s capability in modeling spatial locality. This architecture enables LAformer to effectively integrate local and global information, enhancing its representational power. Notably, LAformer circumvents hardware-inefficient operations like softmax and window shifting, significantly boosting its efficiency for high-resolution image processing. As shown in Fig. 1, our LAformer surpasses SOTA Transformer-based IR methods and significantly reduces computational overhead.

Our main contributions can be summarized as follows:

- We propose LAformer, a simple, efficient, and strong model that combines powerful representation capability with linear complexity. To the best of our knowledge, this is the first work to demonstrate the effectiveness of linear attention in high-resolution image restoration tasks.
- We propose Rank Enhanced Linear Attention (RELA), a

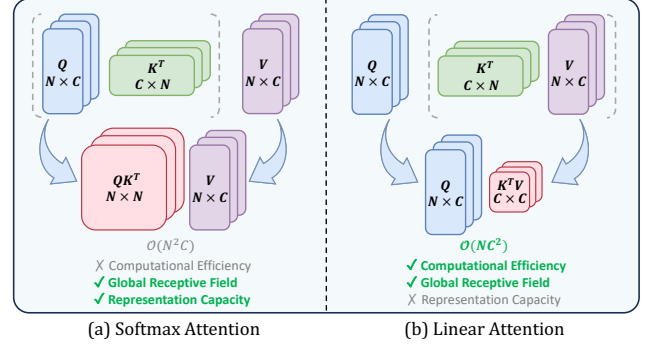


Figure 2. Conceptual comparison between **Softmax Attention** and **Linear Attention**. Instead of using softmax, linear attention employs simpler activation functions (e.g., ReLU) to decouple the process, altering the computation order to first calculate $K^T V$. While linear attention excels at efficiently capturing global context, its representation capacity is limited compared to softmax attention, resulting in a notable performance drop.

simple yet effective mechanism that boosts feature diversity in linear attention by enhancing the rank of features.

- Extensive experiments across 7 tasks and 21 benchmarks demonstrate that LAformer achieves state-of-the-art performance while maintaining high efficiency.

2. Related Work

Image Restoration. Images captured in real-world scenarios often suffer from various degradations, such as blur, low-light, and adverse weather conditions. These issues inevitably degrade the performance of downstream models and diminish the effectiveness of many vision systems [63, 131]. SRCNN [25] and DnCNN [121] are pioneering works that introduce CNN into image restoration and achieve impressive results. Subsequently, a plethora of CNN-based architectures incorporating meticulously designed modules have been introduced to enhance IR performance. Notable examples include the residual block [37, 42, 51], dense block [95, 125, 127], channel attention [124], and non-local attention mechanisms [65, 66, 102]. Despite their success, CNNs remain constrained by their inherently limited receptive field, posing challenges in effectively capturing long-range dependencies. Recently, researchers have begun to use self-attention mechanisms in place of convolutions to enhance IR performance [12, 50, 98, 115].

Vision Transformer. Since its introduction by NLP researchers, Transformer [92] has been widely adopted in computer vision tasks [27, 58, 94]. IPT [12] is the pioneering work that introduces Transformer to image restoration by processing images in small patches. Since then, many works [49, 115, 123] have focused on improving self-attention, aiming to reduce its significant computational overhead. SwinIR [50] and Uformer [98] perform self-attention in non-overlapping local windows. HAT [17] pro-

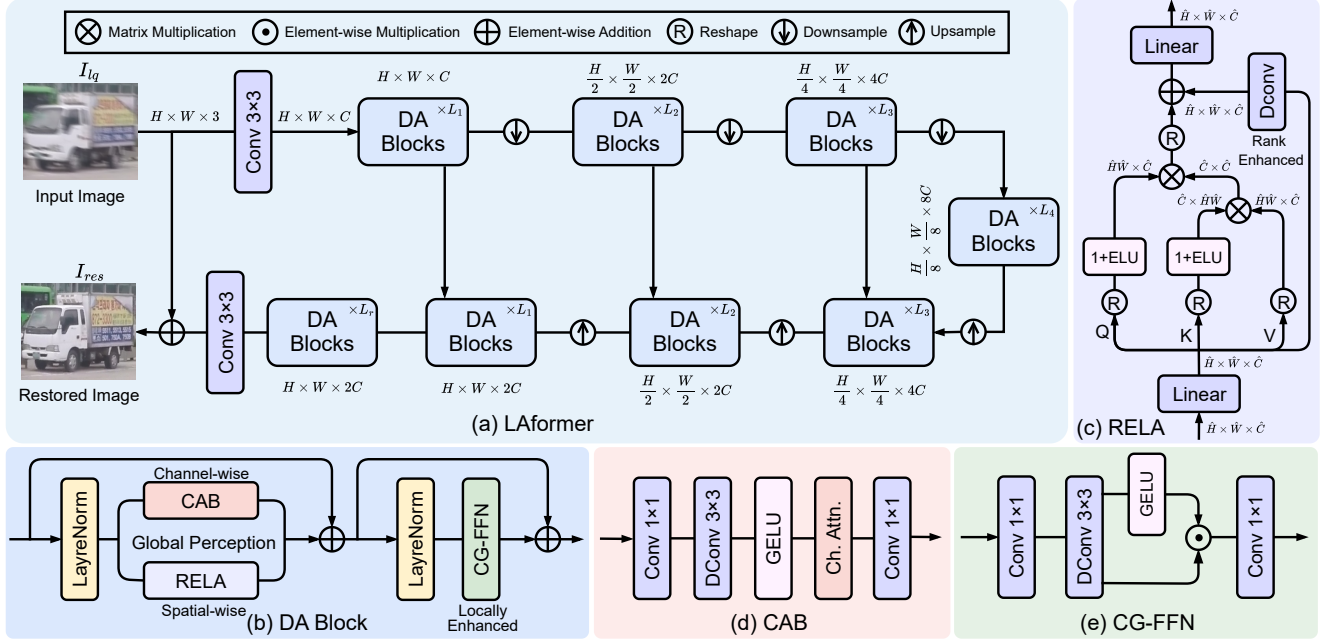


Figure 3. Overall architecture of the proposed LAformer, which includes (b) Dual Attention (DA) Block, (c) Rank Enhanced Linear Attention (RELA), (d) Channel Attention Block (CAB), and (e) Convolutional-Gated Feed-Forward Network (CG-FFN).

poses overlapping cross-attention to establish cross-window interaction. ART [120] introduces sparse attention to IR for a large receptive field. AST [129] proposes an adaptive sparse self-attention to filter out irrelevant tokens. Although effective, a trade-off between global receptive field and computational efficiency persists.

Linear attention [36] substitutes the softmax operation with separate activation functions and reduces complexity from quadratic to linear by reordering the computation of Q , K , and V . Due to its efficiency and ability to capture global context, it has garnered significant interest from the computer vision community. Shen *et al.* [82] introduce linear attention to object detection and instance segmentation. Bolya *et al.* [7] propose hydra attention by maximizing the number of linear attention heads. Han *et al.* [32] propose a focused linear attention module to enhance efficiency and expressiveness. Recently, EfficientViT [9] finds that linear attention cannot produce sharp attention distributions and proposes multi-scale linear attention to enhance local information extraction. Sana [105] extends EfficientViT to Diffusion Transformer [70] to facilitate high-resolution image generation. Distinct from prior works, ours is the first to demonstrate the efficacy of linear attention in high-resolution image restoration. Additionally, we investigate the limitation of linear attention in representation capacity and propose novel approaches to overcome the challenge.

3. Method

We propose LAformer, an efficient framework for high-resolution IR. First, we analyze the softmax attention and

linear attention mechanisms in Sec. 3.1. Then Sec. 3.2 delves into the inherent low-rank characteristics of linear attention, motivating the development of Rank Enhanced Linear Attention (RELA) as a solution. Finally, in Sec. 3.3, we present LAformer, a model built on RELA that achieves explicit global modeling with linear complexity.

3.1. Softmax vs. Linear Attention

Softmax attention [92] is a widely used mechanism in Transformer. For a given input $X \in \mathbb{R}^{N \times C_{in}}$, where N represents the number of visual tokens and C_{in} denotes the channel dimension, it can be generally formulated as

$$Y_i = \sum_{j=1}^N \frac{\text{Sim}(Q_i, K_j)}{\sum_{s=1}^N \text{Sim}(Q_i, K_s)} V_j, \quad (1)$$

where $Q = XW_Q, K = XW_K, V = XW_V, W_{Q,K,V} \in \mathbb{R}^{C_{in} \times C}$ are learnable linear projection matrices, $\text{Sim}(\cdot, \cdot)$ is the similarity function. When the similarity function is set as $\text{Sim}(Q_i, K_j) = \exp(\frac{Q_i K_j^T}{\sqrt{C}})$, Eq. (1) represents the standard softmax attention. Due to the need to compute similarities between all queries and keys, softmax attention incurs a $\mathcal{O}(N^2)$ complexity.

Linear attention [36] uses simple activation functions to approximate the similarity function as $\text{Sim}(Q_i, K_j) = \psi(Q_i) \psi(K_j)^T$, where $\psi(\cdot)$ is the activation function. With

this assumption, we can rewrite Eq. (1) as

$$Y_i = \sum_{j=1}^N \frac{\psi(Q_i)\psi(K_j)^T}{\sum_{s=1}^N \psi(Q_i)\psi(K_s)^T} V_j$$

$$= \frac{\psi(Q_i) \left(\sum_{j=1}^N \psi(K_j)^T V_j \right)}{\psi(Q_i) \left(\sum_{s=1}^N \psi(K_s)^T \right)}. \quad (2)$$

Compared to softmax attention, linear attention modifies the computation order from $(QK^T)V$ to $Q(K^TV)$, reducing the complexity from $\mathcal{O}(N^2)$ to $\mathcal{O}(N)$ while preserving the global modeling capabilities. However, the improvement in computational efficiency is accompanied by a noticeable drop in performance (See Tab. 11).

3.2. Rank Enhanced Linear Attention

Following [49], we conduct rank analysis for the linear attention map M , which is computed as $\psi(Q)\psi(K)^T \in \mathbb{R}^{N \times N}$. According to basic matrix theory, it follows that

$$\begin{aligned} \text{Rank}(M) &\leq \min(\text{Rank}(\psi(Q)), \text{Rank}(\psi(K)^T)) \\ &\leq \min(N, C). \end{aligned} \quad (3)$$

For high-resolution IR, the number of visual tokens N is typically much larger than the number of channels C , which results in the low-rank nature of the attention map in linear attention. Since the attention output is a weighted sum of V using the attention map, the highly correlated weights inevitably limit the expressive capacity of the output features. As shown in Fig. 4, the rank of output features produced by linear attention is notably lower than that of softmax attention, suggesting a reduced diversity in features.

To address this limitation, we introduce Rank Enhanced Linear Attention (RELA), depicted in Fig. 3 (c). We integrate a lightweight depth-wise convolution into the computation process, which can be formulated as

$$Y = (1 + \text{ELU}(Q))(1 + \text{ELU}(K))^T V + W_d V, \quad (4)$$

where W_d represents the depth-wise convolution. Following [36], we use $1 + \text{ELU}(\cdot)$ as the activation function.

The depth-wise convolution can be interpreted as a local attention operation, enriching the output through local feature combinations, thereby alleviating the low-rank limitations of global attention weighting. Fig. 4 illustrates that our RELA successfully restores the output features to a full-rank state, substantially enhancing the diversity of learned features. We further perform a rank analysis across all model blocks, with additional details provided in Fig. 7 of Sec. 4.3. It is worth noting that our RELA introduces only a minimal increase in parameters and computational overhead compared to standard linear attention, yet it brings a significant performance boost (See Tab. 11). More analysis is provided in the Appendix.

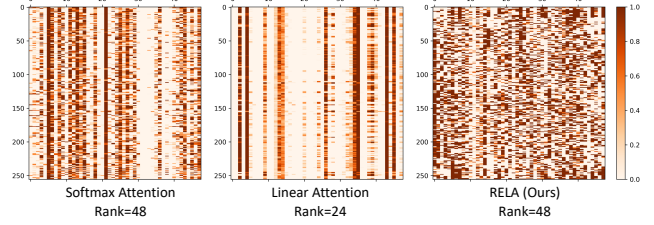


Figure 4. Comparison of feature maps ($N = 256, C = 48$) output by softmax attention (window-based), linear attention, and RELA. The output features of linear attention often exhibit pronounced low-rank characteristics, which constrain its representational capacity. Our proposed RELA mitigates this limitation, substantially enriching the expressiveness of the resulting features.

3.3. Network Architecture

3.3.1. Overall Architecture

The overall architecture of our LAformer is depicted in Fig. 3. To rigorously assess the effectiveness of our proposed method, we adopt the classical U-Net architecture as the backbone, aligning with previous approaches [13, 98, 115]. For an input low-quality (LQ) image $I_{lq} \in \mathbb{R}^{H \times W \times 3}$, LAformer initially applies a 3×3 convolution for overlapping patch embedding, transforming I_{lq} into a feature map with C channels. In both the encoder and decoder modules, we incorporate Dual Attention (DA) Blocks to efficiently capture both global and local degradation patterns. Within each stage, skip connections link the encoder and decoder, enabling seamless information flow across intermediate features. Across stages, pixel-unshuffle and pixel-shuffle operations are employed for effective feature down-sampling and up-sampling. All learnable parameters are optimized using the L_1 loss, calculated between the restored image I_{res} and the ground truth image I_{gt} .

3.3.2. Dual Attention Block

To improve both global and local feature extraction in LAformer, we integrate a dual attention module and a Convolutional Gated Feed-Forward Network (CG-FFN), which address global and local feature learning, respectively. The details of these components are outlined below.

Dual Attention. We use the proposed RELA to achieve efficient global modeling in the spatial dimension. Considering that channel-wise information also plays an important role in IR, we introduce channel attention [124] into the DA Block, forming the Channel Attention Block (CAB) in conjunction with convolutions, as depicted in Fig. 3 (d). The process of CAB can be formulated as

$$Y = W_{p_2} \text{CA}(\text{GELU}(W_d W_{p_1} X)), \quad (5)$$

where W_{p_1} is the 1×1 point-wise convolution, W_d is the 3×3 depth-wise convolution, $\text{CA}(\cdot)$ denotes the channel attention operation. Channel attention can be interpreted as a mechanism for modeling global dependencies,

Dataset	Method	DeblurGAN-v2 [41]	SRN [87]	MIMO-Unet+ [20]	MPRNet [114]	DeepRFT+ [89]	BANet [38]	MSSNet [64]	Stripformer [88]	FFTformer [39]	GRL [49]	LAformer-B Ours
RealBlur-R [79]	PSNR	36.44	38.65	N/A	39.31	39.55	39.76	39.84	39.84	40.11	40.20	41.07
	SSIM	0.935	0.965	N/A	0.972	0.971	0.972	0.972	0.974	0.973	0.974	0.977
RealBlur-J [79]	PSNR	29.69	31.38	31.92	31.76	32.00	32.10	32.19	32.48	32.62	32.82	32.92
	SSIM	0.870	0.909	0.919	0.922	0.923	0.928	0.931	0.929	0.933	0.932	0.933

Table 1. **Motion deblurring** results on real-world datasets. All models are trained and tested on RealBlur [79].

Method	Venue	GoPro [67]		HIDE [81]	
		PSNR ↑	SSIM ↑	PSNR ↑	SSIM ↑
DeblurGAN [40]	CVPR'18	28.70	0.858	24.51	0.871
Nah <i>et al.</i> [67]	CVPR'17	29.08	0.914	25.73	0.874
Zhang <i>et al.</i> [118]	ICCV'18	29.19	0.931	N/A	N/A
DeblurGAN-v2 [41]	ICCV'19	29.55	0.934	26.61	0.875
SRN [87]	CVPR'18	30.26	0.934	28.36	0.915
Gao <i>et al.</i> [29]	CVPR'19	30.90	0.935	29.11	0.913
DBGAN [122]	CVPR'20	31.10	0.942	28.94	0.915
MT-RNN [69]	ECCV'20	31.15	0.945	29.15	0.918
DMPHN [117]	CVPR'19	31.20	0.940	29.09	0.924
Suin <i>et al.</i> [85]	CVPR'20	31.85	0.948	29.98	0.930
MIMO-Unet+ [20]	ICCV'21	32.45	0.957	29.99	0.930
IPT [12]	CVPR'21	32.52	N/A	N/A	N/A
MPRNet [114]	CVPR'21	32.66	0.959	30.96	0.939
Restormer [93]	CVPR'22	32.92	0.961	31.22	0.942
Stripformer [88]	ECCV'22	33.08	0.962	31.03	0.940
HI-Diff [19]	NIPS'23	33.33	0.964	31.46	0.945
IRNeXt [23]	ICML'23	33.16	0.962	N/A	N/A
PromptRestorer [93]	NIPS'23	33.06	0.962	31.36	0.944
FPro [130]	ECCV'24	33.05	0.961	N/A	N/A
LAformer-B	-	33.40	0.965	31.49	0.945

Table 2. **Motion deblurring** results on synthetic datasets. All models are only trained on the GoPro [67] dataset.

as it aggregates token information across the spatial domain through global average pooling. In the DA Block, we combine RELA and CAB to effectively model and aggregate global information across both spatial and channel dimensions, achieving efficient global modeling and aggregation.

Convolutional Gated FFN. As discussed in [9], compared to softmax attention, linear attention tends to produce less sharp attention maps, which hinders its ability to effectively capture local information. However, rich local information is crucial for restoring texture details. To address this, we propose a simple Convolutional Gated Feed-Forward Network (CG-FFN) to enhance the local fitting capability of LAformer. As illustrated in Fig. 3 (e), CG-FFN integrates depth-wise convolution with Gated Linear Unit (GLU) [24], which can be formulated as

$$Y = W_{p_2}(\text{GELU}(W_d W_{p_1} X) \odot W_d W_{p_1} X). \quad (6)$$

Compared to MLP, CG-FFN incorporates depth-wise convolution to enhance LAformer’s capacity for capturing fine-grained local details while reducing computational cost, thereby complementing the linear attention mechanism.

Dual-Attention Block. Our DA Block is equipped with RELA, CAB, and CG-FFN, which is defined as

$$\begin{aligned} X' &= \text{RELA}(\text{LN}(X)) + \text{CAB}(\text{LN}(X)) + X, \\ Y &= \text{CGFFN}(\text{LN}(X')) + X'. \end{aligned} \quad (7)$$

Built upon the stacked DA Blocks, LAformer avoids hardware-inefficient operations (*e.g.*, softmax, window

Method	Uformer [98]	Restormer [115]	Stripformer [88]	HI-Diff [19]	LAformer-B Ours
#Params (M)	50.88	26.13	19.71	28.49	24.89
FLOPs (G)	86.89	154.88	155.03	142.62	144.33
Runtime (s)	1.41	0.79	0.87	1.56	0.76
PSNR (dB)	32.97	32.96	33.08	33.33	33.40

Table 3. **Model efficiency** comparison with SOTA Transformer-based methods on the GoPro [67] dataset (1280 × 720 resolution).

shifting) and explicitly models spatial-wise global features, channel-wise global features, and local features, all with linear complexity. This enables LAformer to maintain high efficiency while possessing strong representation capability.

4. Experiments

4.1. Experimental Setup

We evaluate the proposed LAformer on various datasets for 7 image restoration tasks: (1) motion deblurring, (2) defocus deblurring, (3) image dehazing, (4) image desnowing, (5) raindrop removal, (6) low-light enhancement, and (7) all-in-one image restoration. Additional details about the training dataset, training protocols, and more visual results can be found in the Appendix due to space limits.

Implementation Details. We optimize LAformer using the AdamW optimizer ($\beta_1 = 0.9, \beta_2 = 0.999$) with L_1 loss. Data augmentation includes random rotations, flipping, and cropping. The initial learning rate is set to 3×10^{-4} , which is gradually decayed to 1×10^{-6} using the cosine annealing scheduler. The progressive training strategy [115] is employed to reduce training time. The kernel size for the depth-wise convolution in RELA is set to 5×5 . To align with SOTA models for each specific task, we adapt the number of blocks and channels, considering variants of different sizes, including Tiny, Small, and Base versions (LAformer-T/S/B). The training of LAformer is conducted on 8 NVIDIA V100 GPUs. Additional task-specific training hyperparameters and details of the model architecture can be found in the Appendix.

4.2. Main Results

Motion Deblurring. Tab. 2 and Tab. 1 show the motion deblurring results on the synthetic and real-world datasets, respectively. When trained on the synthetic GoPro [67] dataset, our model outperforms all comparison methods on both the GoPro and HIDE [81] datasets. When trained on the real RealBlur [79] dataset, our model achieves the best results, surpassing GRL [49] by 0.87 dB in PSNR on RealBlur-R. Fig. 5 shows that LAformer produces sharper



Figure 5. Top row: Visual comparison on the DPDD [1] dataset for **single-image defocus deblurring**. Bottom row: Visual comparison on the GoPro [67] dataset for **motion deblurring**. Zoom in for a better view.

Method	Indoor Scenes				Outdoor Scenes				Combined			
	PSNR \uparrow	SSIM \uparrow	MAE \downarrow	LPIPS \downarrow	PSNR \uparrow	SSIM \uparrow	MAE \downarrow	LPIPS \downarrow	PSNR \uparrow	SSIM \uparrow	MAE \downarrow	LPIPS \downarrow
EBDB _S [35]	25.77	0.772	0.040	0.297	21.25	0.599	0.058	0.373	23.45	0.683	0.049	0.336
DMENet _S [43]	25.50	0.788	0.038	0.298	21.43	0.644	0.063	0.397	23.41	0.714	0.051	0.349
JNB _S [83]	26.73	0.828	0.031	0.273	21.10	0.608	0.064	0.355	23.84	0.715	0.048	0.315
DPDNet _S [1]	26.54	0.816	0.031	0.239	22.25	0.682	0.056	0.313	24.34	0.747	0.044	0.277
KPAC _S [84]	27.97	0.852	0.026	0.182	22.62	0.701	0.053	0.269	25.22	0.774	0.040	0.227
IFAN _S [44]	28.11	0.861	0.026	0.179	22.76	0.720	0.052	0.254	25.37	0.789	0.039	0.217
DRBNet _S [80]	N/A	N/A	N/A	N/A	N/A	N/A	N/A	N/A	25.73	0.791	N/A	0.183
Restormer _S [115]	<u>28.87</u>	<u>0.882</u>	<u>0.025</u>	<u>0.145</u>	<u>23.24</u>	<u>0.743</u>	<u>0.050</u>	<u>0.209</u>	25.98	<u>0.811</u>	<u>0.038</u>	<u>0.178</u>
NRKNet _S [76]	N/A	N/A	N/A	N/A	N/A	N/A	N/A	N/A	<u>26.11</u>	0.810	N/A	0.210
INIKNet _S [77]	N/A	N/A	N/A	N/A	N/A	N/A	N/A	N/A	26.05	0.803	N/A	0.185
MPerceiver _S [4]	N/A	N/A	N/A	N/A	N/A	N/A	N/A	N/A	25.88	0.803	N/A	0.190
LAformer-B_S	29.13	0.886	0.024	<u>0.146</u>	23.57	0.759	0.048	0.207	26.28	0.821	0.036	0.177
DPDNet _D [1]	27.48	0.849	0.029	0.189	22.90	0.726	0.052	0.255	25.13	0.786	0.041	0.223
RDPD _D [2]	28.10	0.843	0.027	0.210	22.82	0.704	0.053	0.298	25.39	0.772	0.040	0.255
Uformer _D [98]	28.23	0.860	0.026	0.199	23.10	0.728	0.051	0.285	25.65	0.795	0.039	0.243
IFAN _D [44]	28.66	0.868	0.025	0.172	23.46	0.743	0.049	0.240	25.99	0.804	0.037	0.207
Restormer _D [115]	29.48	<u>0.895</u>	<u>0.023</u>	<u>0.134</u>	<u>23.97</u>	<u>0.773</u>	<u>0.047</u>	<u>0.175</u>	<u>26.66</u>	<u>0.833</u>	<u>0.035</u>	<u>0.155</u>
LAformer-B_D	29.53	0.898	0.023	0.125	24.49	0.795	0.044	0.160	26.95	0.845	0.034	0.143

Table 4. **Defocus deblurring** results on the DPDD testset [1]. **S**: single-image defocus deblurring. **D**: dual-pixel defocus deblurring.

Method	SOTS-Indoor [46]		SOTS-Outdoor [46]	
	PSNR \uparrow	SSIM \uparrow	PSNR \uparrow	SSIM \uparrow
DCP [33]	16.62	0.818	19.13	0.815
DehazeNet [8]	19.82	0.821	24.75	0.927
AOD-Net [45]	20.51	0.816	24.14	0.920
GridDehazeNet [54]	32.16	0.984	30.86	0.982
MSBDN [26]	33.67	0.985	33.48	0.982
FFA-Net [73]	36.39	0.989	33.57	0.984
AECC-Net [100]	37.17	0.990	N/A	N/A
MAXIM [90]	38.11	0.991	34.19	0.985
DeHamer [31]	36.63	0.988	35.18	0.986
PMNet [110]	38.41	0.990	34.74	0.985
FocalNet [22]	<u>40.82</u>	<u>0.996</u>	<u>37.71</u>	<u>0.995</u>
MB-TaylorFormer [74]	40.71	0.992	37.42	0.989
LAformer-T	41.17	0.996	38.51	0.995

Table 5. **Image dehazing** results on synthetic datasets.

Method	Outdoor-Haze [5]		Dense-Haze [6]	
	PSNR \uparrow	SSIM \uparrow	PSNR \uparrow	SSIM \uparrow
DCP [33]	16.78	0.653	12.72	0.442
DehazeNet [8]	17.57	0.770	13.84	0.430
AOD-Net [45]	15.03	0.540	13.14	0.410
GridDehazeNet [54]	18.92	0.672	14.96	0.536
MSBDN [26]	24.36	0.749	15.13	0.555
FFA-Net [73]	22.12	0.770	15.70	0.549
AECC-Net [100]	N/A	N/A	15.80	0.470
Restormer [115]	23.58	0.768	15.78	0.548
DeHamer [31]	<u>25.11</u>	0.777	16.62	0.560
PMNet [110]	24.64	<u>0.830</u>	16.79	0.510
MB-TaylorFormer [74]	25.05	0.788	16.66	<u>0.560</u>
AST [129]	N/A	N/A	<u>17.12</u>	0.550
LAformer-T	25.28	0.932	17.14	0.565

Table 6. **Image dehazing** results on real-world datasets.

and clearer results compared to other methods.

We present a comparison of model efficiency on the GoPro dataset in Tab. 3, where FLOPs are computed using 256×256 input images. Notably, our method demonstrates more than a twofold speedup over the recent SOTA HI-Diff [19], while delivering superior PSNR performance. This result underscores the powerful capability of LAformer in high-resolution IR, achieving a compelling balance of performance and efficiency.

Defocus Deblurring. Tab. 4 shows the comparison re-

sults on the DPDD [1] dataset. Our LAformer consistently outperforms SOTA methods across all three scene types. Specifically, in the combined scenes, LAformer achieves a PSNR improvement of 0.3 dB over the Transformer-based method Restormer [115] in the single-image setting, and a 0.29 dB improvement in the dual-pixel setting. Fig. 5 shows that LAformer restores clear text, whereas other methods result in noticeable blurring or artifacts.

Image Dehazing. Tab. 5 and Tab. 6 present the dehazing results on the synthetic and real-world datasets, respectively.

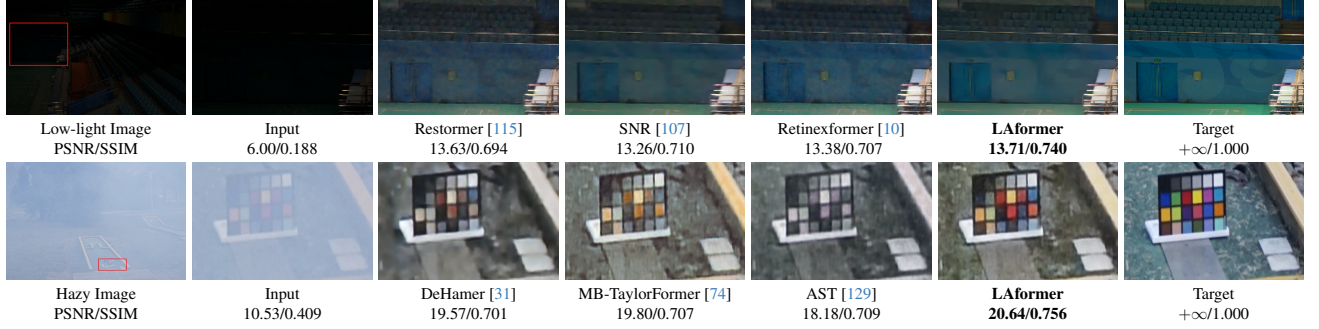


Figure 6. Top row: Visual comparison on the LOL-v1 [99] dataset for **low-light enhancement**. Bottom row: Visual comparison on the Dense-Haze [6] dataset for **image dehazing**. Zoom in for a better view.

Method	CSD [15]		SRRS [14]		Snow100K [57]	
	PSNR	SSIM	PSNR	SSIM	PSNR	SSIM
DesnowNet [57]	20.13	0.81	20.38	0.84	30.50	0.94
CycleGAN [28]	20.98	0.80	20.21	0.74	26.81	0.89
All in One [48]	26.31	0.87	24.98	0.88	26.07	0.88
JSTASR [14]	27.96	0.88	25.82	0.89	23.12	0.86
HDCW-Net [15]	29.06	0.91	27.78	0.92	31.54	0.95
TransWeather [91]	31.76	0.93	28.29	0.92	31.82	0.93
NAFNet [13]	33.13	0.96	29.72	0.94	32.41	0.95
FocalNet [22]	<u>37.18</u>	<u>0.99</u>	<u>31.34</u>	<u>0.98</u>	<u>33.53</u>	<u>0.95</u>
LAformer-T	37.42	0.99	32.24	0.98	34.24	0.96

Table 7. **Image desnowing** results on three widely used datasets.

Method	Venue	Test-A		Test-B	
		PSNR	SSIM	PSNR	SSIM
pix2pix [34]	CVPR'18	28.02	0.855	N/A	N/A
AGAN [72]	CVPR'18	31.62	0.921	25.05	0.811
Quan <i>et al.</i> [75]	ICCV'19	31.44	0.926	N/A	N/A
DuRN [55]	CVPR'19	31.24	0.926	25.32	0.817
Restormer [115]	CVPR'22	32.18	0.941	N/A	N/A
MAXIM [90]	CVPR'22	31.87	0.935	<u>25.74</u>	<u>0.827</u>
IDT [104]	TPAMI'23	31.87	0.931	N/A	N/A
WeatherDiff [68]	TAPMI'23	32.43	0.933	N/A	N/A
AWRCP [111]	ICCV'23	31.93	0.931	N/A	N/A
DTPM [112]	CVPR'24	32.72	0.944	N/A	N/A
AST [129]	CVPR'24	32.32	0.935	N/A	N/A
Histoformer [86]	ECCV'24	<u>33.06</u>	<u>0.944</u>	N/A	N/A
LAformer-S	-	33.38	0.949	27.27	0.850

Table 8. **Raindrop removal** results on the Raindrop [72] dataset.

LAformer achieves the best performance for all datasets. Fig. 6 shows that LAformer achieves the dehazing result closest to the ground truth compared to other methods.

Image Desnowing. Tab. 7 shows the desnowing results on three widely used datasets. We follow the dataset split used in FocalNet [22]. Our method achieves the best performance across three datasets.

Raindrop Removal. Tab. 8 shows the raindrop removal results on the Raindrop [72] dataset. Compared to recent methods AST [129] and Histoformer [86], LAformer achieves a PSNR gain of 1.06 dB and 0.32 dB, respectively.

Low-light Enhancement. As shown in Tab. 9, LAformer achieves the best PSNR score for all datasets. Fig. 6 shows that LAformer produces the clearest visual results, while the results of the comparative methods contain noticeable noise and artifacts.

Method	LOL-v1 [99]		LOL-v2-real [109]		LOL-v2-syn [109]	
	PSNR	SSIM	PSNR	SSIM	PSNR	SSIM
SID [11]	14.35	0.436	13.24	0.442	15.04	0.610
IPT [12]	16.27	0.504	19.80	0.813	18.30	0.811
Uformer [98]	16.36	0.771	18.82	0.771	19.66	0.871
Sparse [109]	17.20	0.640	20.06	0.816	22.05	0.905
RUAS [53]	18.23	0.720	18.37	0.723	16.55	0.652
SCI [62]	14.78	0.646	20.28	0.752	24.14	0.928
KinD [126]	20.87	0.802	17.54	0.669	13.29	0.578
MIRNet [113]	24.14	0.830	20.02	0.820	21.94	0.876
DRBN [108]	19.86	0.834	20.13	0.830	23.22	0.827
URetInex-Net [101]	21.33	0.835	21.16	0.840	24.14	0.928
Restormer [115]	22.43	0.823	19.94	0.827	21.41	0.830
MRQ [56]	25.24	0.855	22.37	0.846	25.94	0.935
LLFlow [97]	25.19	0.870	26.53	0.892	26.23	<u>0.943</u>
SNR [107]	24.61	0.842	23.92	0.849	25.77	0.894
Retinexformer [10]	<u>27.18</u>	0.850	<u>27.71</u>	0.856	<u>29.04</u>	0.939
LAformer-T	27.28	<u>0.868</u>	27.92	<u>0.868</u>	30.28	0.952

Table 9. **Low-light enhancement** results on three datasets.

All-in-One IR. We further validate the effectiveness of LAformer on the all-in-one IR task. Following the five-task setting of DiffUIR [128], we train a single LAformer model to address five different types of degradations. As shown in Tab. 10, our LAformer outperforms DiffUIR across all tasks, delivering significant performance gains. This further highlights the strong representation capacity of LAformer, which achieves superior results without requiring any specialized design for the all-in-one IR task.

4.3. Ablation Study

As shown in Tab. 11 and Tab. 12, we perform detailed ablation studies on SOTS-Indoor [46] and GoPro [67] datasets to analyze the role of each component in LAformer. For fair comparisons, all models are designed with comparable complexity. FLOPs are computed on 256×256 images. More ablations and analysis are provided in the Appendix.

Rank Enhanced Linear Attention. As shown in Tab. 11, RELA significantly improves performance over vanilla linear attention, achieving a 1.89 dB PSNR gain on SOTS-Indoor with only a modest increase of 0.07M parameters and 0.76G FLOPs. We also compare RELA with the commonly used window self-attention [50] and transposed self-attention [115] in image restoration. With similar parameter

Method	Venue	Deraining (5sets)		Enhancement		Desnowing (2sets)		Dehazing		Deblurring	
		PSNR \uparrow	SSIM \uparrow	PSNR \uparrow	SSIM \uparrow	PSNR \uparrow	SSIM \uparrow	PSNR \uparrow	SSIM \uparrow	PSNR \uparrow	SSIM \uparrow
Task-Specific											
SwinIR [50]	ICCVW'21	N/A	N/A	17.81	0.723	N/A	N/A	21.50	0.891	24.52	0.773
MIRNetV2 [116]	TPAMI'22	N/A	N/A	24.74	0.851	N/A	N/A	24.03	0.927	26.30	0.799
IR-SDE [60]	ICML'23	N/A	N/A	20.45	0.787	N/A	N/A	N/A	N/A	<u>30.70</u>	<u>0.901</u>
WeatherDiff [68]	TPAMI'23	N/A	N/A	N/A	N/A	<u>33.51</u>	<u>0.939</u>	N/A	N/A	N/A	N/A
RDDM [52]	CVPR'24	30.74	0.903	23.22	0.899	32.55	0.927	30.78	0.953	29.53	0.876
All-in-One											
Restormer [115]	CVPR'22	27.10	0.843	17.63	0.542	28.61	0.876	22.79	0.706	26.36	0.814
AirNet [47]	CVPR'22	24.87	0.773	14.83	0.767	27.63	0.860	25.47	0.923	26.92	0.811
Painter [96]	CVPR'23	29.49	0.868	22.40	0.872	N/A	N/A	N/A	N/A	N/A	N/A
IDR [119]	CVPR'23	N/A	N/A	21.34	0.826	N/A	N/A	25.24	0.943	27.87	0.846
ProRes [61]	arXiv'23	30.67	0.891	22.73	0.877	N/A	N/A	N/A	N/A	27.53	0.851
PromptIR [71]	NeurIPS'23	29.56	0.888	22.89	0.847	31.98	0.924	32.02	0.952	27.21	0.817
DACLIP [59]	ICLR'24	28.96	0.853	24.17	0.882	30.80	0.888	31.39	<u>0.983</u>	25.39	0.805
DiffUIR [128]	CVPR'24	<u>31.03</u>	<u>0.904</u>	<u>25.12</u>	<u>0.907</u>	32.65	0.927	<u>32.94</u>	0.956	29.17	0.864
LAformer-B	-	31.55	0.914	26.81	0.924	34.24	0.942	34.28	0.984	30.92	0.910

Table 10. All-in-one image restoration results for five tasks. We strictly follow the setting of DiffUIR [128].

Method	#Params (M)	FLOPs (G)	PSNR (dB)
Vanilla LA [36]	6.18	29.08	39.28
Window SA [50]	6.20	30.19	40.76
Transposed SA [115]	6.26	29.87	40.52
Rank Enhanced LA	6.25	29.84	41.17
w/o CAB	6.13	30.79	40.81
Dual Attention	6.25	29.84	41.17
MLP	6.59	30.96	40.20
CG-FFN w/o DWC	6.24	30.16	40.11
CG-FFN w/o GLU	6.28	29.60	40.86
CG-FFN	6.25	29.84	41.17

Table 11. Ablations on SOTS-Indoor [46] for LAformer-T.

RELA	Params (M)	FLOPs (G)	PSNR (dB)
$\psi(\cdot) = \text{ReLU}(\cdot)$	24.89	144.33	33.38
$\psi(\cdot) = 1 + \text{ELU}(\cdot)$	24.89	144.33	33.40
3×3 DWC	24.79	143.11	33.35
5×5 DWC	24.89	144.33	33.40
7×7 DWC	25.03	146.16	33.41

Table 12. Ablations on GoPro [67] for RELA designs.

counts and FLOPs, our RELA achieves a PSNR improvement of 0.41 dB and 0.65 dB, respectively. This demonstrates the global perception capability of RELA, which contributes to improved restoration performance.

We also conduct ablations on the design of RELA, as shown in Tab. 12. We analyze the choice of activation function $\psi(\cdot)$, with experimental results indicating minimal impact on PSNR performance. This suggests that the effectiveness of our RELA is not dependent on meticulously chosen activation functions. We further analyze the impact of the depth-wise convolution (DWC) kernel size on the results. Considering both computational efficiency and performance, we ultimately select a 5×5 kernel.

To further validate the rank-enhancing effect of RELA, we conduct rank analysis across model blocks for different attention mechanisms, as shown in Fig. 7. The softmax attention is implemented using window attention [50].

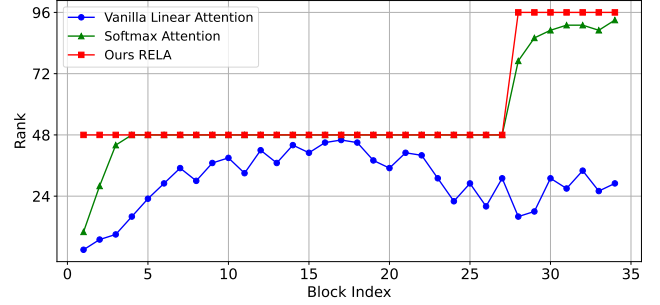


Figure 7. Rank analysis across model blocks for different attention mechanisms. The full rank is 48 for Block₁ to Block₂₇, and 96 for Block₂₈ to Block₃₄.

The output features of linear attention maintain a low rank across most blocks. In contrast, our RELA restores these features to a full-rank state, enhancing the representation capacity of linear attention and thereby improving restoration performance. More rank analysis is provided in the Appendix.

Channel Attention Block. Tab. 11 shows that removing CAB results in a 0.36 dB drop in PSNR, highlighting the importance of channel-wise global information for IR.

Convolutional Gated FFN. Tab. 11 indicates that the DWC in CG-FFN significantly enhances LAformer’s ability to extract local information, markedly improving model performance. Removing the DWC results in nearly a 1 dB drop in PSNR.

5. Conclusion

In this paper, we introduce linear attention to image restoration, aiming to overcome the complexity limitations of Transformer. By performing rank analysis on the feature representations, we uncover the inherent low-rank limitations of vanilla linear attention. To address this, we propose a simple yet effective solution: Rank Enhanced Linear Attention (RELA). RELA enhances the rank of features

through a lightweight depth-wise convolution, thereby improving its representation capability. Building upon RELA, we introduce LAformer, an image restoration Transformer designed to achieve effective global perception through the integration of linear attention and channel attention. Additionally, LAformer enhances local fitting capabilities by incorporating a convolutional gated feed-forward network, which improves the model’s ability to capture fine-grained details. Comprehensive experiments show that LAformer surpasses current SOTA methods in performance, while also offering considerable computational efficiency gains.

References

- [1] Abdullah Abuolaim and Michael S Brown. Defocus deblurring using dual-pixel data. In *ECCV*, pages 111–126, 2020. 6
- [2] Abdullah Abuolaim, Mauricio Delbracio, Damien Kelly, Michael S. Brown, and Peyman Milanfar. Learning to reduce defocus blur by realistically modeling dual-pixel data. In *ICCV*, 2021. 6
- [3] AF Agarap. Deep learning using rectified linear units (relu). *arXiv preprint arXiv:1803.08375*, 2018. 2
- [4] Yuang Ai, Huaibo Huang, Xiaoqiang Zhou, Jiexiang Wang, and Ran He. Multimodal prompt perceiver: Empower adaptiveness generalizability and fidelity for all-in-one image restoration. In *CVPR*, pages 25432–25444, 2024. 6
- [5] Codruta O Ancuti, Cosmin Ancuti, Radu Timofte, and Christophe De Vleeschouwer. O-haze: a dehazing benchmark with real hazy and haze-free outdoor images. In *CVPRW*, pages 754–762, 2018. 6
- [6] Codruta O Ancuti, Cosmin Ancuti, Mateu Sbert, and Radu Timofte. Dense-haze: A benchmark for image dehazing with dense-haze and haze-free images. In *ICIP*, pages 1014–1018, 2019. 6, 7
- [7] Daniel Bolya, Cheng-Yang Fu, Xiaoliang Dai, Peizhao Zhang, and Judy Hoffman. Hydra attention: Efficient attention with many heads. In *ECCV*, pages 35–49, 2022. 3
- [8] Bolun Cai, Xiangmin Xu, Kui Jia, Chunmei Qing, and Dacheng Tao. Dehazenet: An end-to-end system for single image haze removal. *TIP*, 25(11):5187–5198, 2016. 6
- [9] Han Cai, Junyan Li, Muyan Hu, Chuang Gan, and Song Han. Efficientvit: Lightweight multi-scale attention for high-resolution dense prediction. In *ICCV*, pages 17302–17313, 2023. 3, 5
- [10] Yuanhao Cai, Hao Bian, Jing Lin, Haoqian Wang, Radu Timofte, and Yulun Zhang. Retinexformer: One-stage retinex-based transformer for low-light image enhancement. In *ICCV*, pages 12504–12513, 2023. 7
- [11] Chen Chen, Qifeng Chen, Minh N Do, and Vladlen Koltun. Seeing motion in the dark. In *ICCV*, pages 3185–3194, 2019. 7
- [12] Hanting Chen, Yunhe Wang, Tianyu Guo, Chang Xu, Yiping Deng, Zhenhua Liu, Siwei Ma, Chunjing Xu, Chao Xu, and Wen Gao. Pre-trained image processing transformer. In *CVPR*, pages 12299–12310, 2021. 2, 5, 7
- [13] Liangyu Chen, Xiaojie Chu, Xiangyu Zhang, and Jian Sun. Simple baselines for image restoration. In *ECCV*, pages 17–33, 2022. 4, 7
- [14] Wei-Ting Chen, Hao-Yu Fang, Jian-Jiun Ding, Cheng-Che Tsai, and Sy-Yen Kuo. Jstasr: Joint size and transparency-aware snow removal algorithm based on modified partial convolution and veiling effect removal. In *ECCV*, pages 754–770, 2020. 7
- [15] Wei-Ting Chen, Hao-Yu Fang, Cheng-Lin Hsieh, Cheng-Che Tsai, I Chen, Jian-Jiun Ding, Sy-Yen Kuo, et al. All snow removed: Single image desnowing algorithm using hierarchical dual-tree complex wavelet representation and contradict channel loss. In *ICCV*, pages 4196–4205, 2021. 7
- [16] Xiang Chen, Hao Li, Mingqiang Li, and Jinshan Pan. Learning a sparse transformer network for effective image deraining. In *CVPR*, pages 5896–5905, 2023. 1
- [17] Xiangyu Chen, Xintao Wang, Jiantao Zhou, Yu Qiao, and Chao Dong. Activating more pixels in image super-resolution transformer. In *CVPR*, pages 22367–22377, 2023. 1, 2
- [18] Zheng Chen, Yulun Zhang, Jinjin Gu, Linghe Kong, Xiaokang Yang, and Fisher Yu. Dual aggregation transformer for image super-resolution. In *ICCV*, pages 12312–12321, 2023. 1
- [19] Zheng Chen, Yulun Zhang, Ding Liu, Jinjin Gu, Linghe Kong, Xin Yuan, et al. Hierarchical integration diffusion model for realistic image deblurring. In *NeurIPS*, 2023. 5, 6
- [20] Sung-Jin Cho, Seo-Won Ji, Jun-Pyo Hong, Seung-Won Jung, and Sung-Jea Ko. Rethinking coarse-to-fine approach in single image deblurring. In *ICCV*, pages 4641–4650, 2021. 5
- [21] Djork-Arné Clevert. Fast and accurate deep network learning by exponential linear units (elus). *arXiv preprint arXiv:1511.07289*, 2015. 2
- [22] Yuning Cui, Wenqi Ren, Xiaochun Cao, and Alois Knoll. Focal network for image restoration. In *ICCV*, pages 13001–13011, 2023. 6, 7
- [23] Yuning Cui, Wenqi Ren, Sining Yang, Xiaochun Cao, and Alois Knoll. Irnext: Rethinking convolutional network design for image restoration. In *ICML*, 2023. 5
- [24] Yann N Dauphin, Angela Fan, Michael Auli, and David Grangier. Language modeling with gated convolutional networks. In *ICLR*, pages 933–941, 2017. 5
- [25] Chao Dong, Chen Change Loy, Kaiming He, and Xiaoou Tang. Image super-resolution using deep convolutional networks. *TPAMI*, 38(2):295–307, 2015. 1, 2
- [26] Hang Dong, Jinshan Pan, Lei Xiang, Zhe Hu, Xinyi Zhang, Fei Wang, and Ming-Hsuan Yang. Multi-scale boosted dehazing network with dense feature fusion. In *CVPR*, pages 2157–2167, 2020. 6
- [27] Alexey Dosovitskiy. An image is worth 16x16 words: Transformers for image recognition at scale. *arXiv preprint arXiv:2010.11929*, 2020. 2
- [28] Deniz Engin, Anil Geng, and Hazim Kemal Ekenel. Cycle-dehaze: Enhanced cyclegan for single image dehazing. In *CVPRW*, pages 825–833, 2018. 7

- [29] Hongyun Gao, Xin Tao, Xiaoyong Shen, and Jiaya Jia. Dynamic scene deblurring with parameter selective sharing and nested skip connections. In *CVPR*, pages 3848–3856, 2019. 5
- [30] Hayit Greenspan. Super-resolution in medical imaging. *The computer journal*, 52(1):43–63, 2009. 1
- [31] Chun-Le Guo, Qixin Yan, Saeed Anwar, Runmin Cong, Wenqi Ren, and Chongyi Li. Image dehazing transformer with transmission-aware 3d position embedding. In *CVPR*, pages 5812–5820, 2022. 6, 7
- [32] Dongchen Han, Xuran Pan, Yizeng Han, Shiji Song, and Gao Huang. Flatten transformer: Vision transformer using focused linear attention. In *ICCV*, pages 5961–5971, 2023. 3
- [33] Kaiming He, Jian Sun, and Xiaoou Tang. Single image haze removal using dark channel prior. *TPAMI*, 33(12):2341–2353, 2010. 6
- [34] Phillip Isola, Jun-Yan Zhu, Tinghui Zhou, and Alexei A Efros. Image-to-image translation with conditional adversarial networks. In *CVPR*, 2017. 7
- [35] Ali Karaali and Claudio Rosito Jung. Edge-based defocus blur estimation with adaptive scale selection. *TIP*, 2017. 6
- [36] Angelos Katharopoulos, Apoorv Vyas, Nikolaos Pappas, and François Fleuret. Transformers are rnns: Fast autoregressive transformers with linear attention. In *ICML*, pages 5156–5165, 2020. 2, 3, 4, 8
- [37] Jiwon Kim, Jung Kwon Lee, and Kyoung Mu Lee. Accurate image super-resolution using very deep convolutional networks. In *CVPR*, pages 1646–1654, 2016. 2
- [38] Kiyeon Kim, Seungyong Lee, and Sunghyun Cho. Msnnet: Multi-scale-stage network for single image deblurring. In *ECCV*, pages 524–539, 2022. 5
- [39] Lingshun Kong, Jiangxin Dong, Jianjun Ge, Mingqiang Li, and Jinshan Pan. Efficient frequency domain-based transformers for high-quality image deblurring. In *CVPR*, pages 5886–5895, 2023. 5
- [40] Orest Kupyn, Volodymyr Budzan, Mykola Mykhailych, Dmytro Mishkin, and Jifí Matas. Deblurgan: Blind motion deblurring using conditional adversarial networks. In *CVPR*, pages 8183–8192, 2018. 5
- [41] Orest Kupyn, Tetiana Martyniuk, Junru Wu, and Zhangyang Wang. Deblurgan-v2: Deblurring (orders-of-magnitude) faster and better. In *ICCV*, pages 8878–8887, 2019. 5
- [42] Christian Ledig, Lucas Theis, Ferenc Huszár, Jose Caballero, Andrew Cunningham, Alejandro Acosta, Andrew Aitken, Alykhan Tejani, Johannes Totz, Zehan Wang, et al. Photo-realistic single image super-resolution using a generative adversarial network. In *CVPR*, pages 4681–4690, 2017. 2
- [43] Junyong Lee, Sungkil Lee, Sunghyun Cho, and Seungyong Lee. Deep defocus map estimation using domain adaptation. In *CVPR*, 2019. 6
- [44] Junyong Lee, Hyeongseok Son, Jaesung Rim, Sunghyun Cho, and Seungyong Lee. Iterative filter adaptive network for single image defocus deblurring. In *CVPR*, pages 2034–2042, 2021. 6
- [45] Boyi Li, Xiulian Peng, Zhangyang Wang, Jizheng Xu, and Dan Feng. Aod-net: All-in-one dehazing network. In *ICCV*, pages 4770–4778, 2017. 6
- [46] Boyi Li, Wenqi Ren, Dengpan Fu, Dacheng Tao, Dan Feng, Wenjun Zeng, and Zhangyang Wang. Benchmarking single-image dehazing and beyond. *TIP*, 28(1):492–505, 2018. 6, 7, 8
- [47] Boyun Li, Xiao Liu, Peng Hu, Zhongqin Wu, Jiancheng Lv, and Xi Peng. All-in-one image restoration for unknown corruption. In *CVPR*, pages 17452–17462, 2022. 8
- [48] Ruoteng Li, Robby T Tan, and Loong-Fah Cheong. All in one bad weather removal using architectural search. In *CVPR*, pages 3175–3185, 2020. 7
- [49] Yawei Li, Yuchen Fan, Xiaoyu Xiang, Denis Demandolx, Rakesh Ranjan, Radu Timofte, and Luc Van Gool. Efficient and explicit modelling of image hierarchies for image restoration. In *CVPR*, pages 18278–18289, 2023. 1, 2, 4, 5
- [50] Jingyun Liang, Jiezhong Cao, Guolei Sun, Kai Zhang, Luc Van Gool, and Radu Timofte. Swinir: Image restoration using swin transformer. In *ICCV*, pages 1833–1844, 2021. 1, 2, 7, 8
- [51] Bee Lim, Sanghyun Son, Heewon Kim, Seungjun Nah, and Kyoung Mu Lee. Enhanced deep residual networks for single image super-resolution. In *CVPRW*, pages 136–144, 2017. 2
- [52] Jiawei Liu, Qiang Wang, Huijie Fan, Yinong Wang, Yandong Tang, and Liangqiong Qu. Residual denoising diffusion models. In *CVPR*, pages 2773–2783, 2024. 8
- [53] Risheng Liu, Long Ma, Jiao Zhang, Xin Fan, and Zhongxuan Luo. Retinex-inspired unrolling with cooperative prior architecture search for low-light image enhancement. In *CVPR*, pages 10561–10570, 2021. 7
- [54] Xiaohong Liu, Yongrui Ma, Zhihao Shi, and Jun Chen. Griddehazenet: Attention-based multi-scale network for image dehazing. In *ICCV*, pages 7314–7323, 2019. 6
- [55] Xing Liu, Masanori Suganuma, Zhun Sun, and Takayuki Okatani. Dual residual networks leveraging the potential of paired operations for image restoration. In *CVPR*, pages 7007–7016, 2019. 7
- [56] Yunlong Liu, Tao Huang, Weisheng Dong, Fangfang Wu, Xin Li, and Guangming Shi. Low-light image enhancement with multi-stage residue quantization and brightness-aware attention. In *ICCV*, pages 12140–12149, 2023. 7
- [57] Yun-Fu Liu, Da-Wei Jaw, Shih-Chia Huang, and Jenq-Neng Hwang. Desnownet: Context-aware deep network for snow removal. *TIP*, 27(6):3064–3073, 2018. 7
- [58] Ze Liu, Yutong Lin, Yue Cao, Han Hu, Yixuan Wei, Zheng Zhang, Stephen Lin, and Baining Guo. Swin transformer: Hierarchical vision transformer using shifted windows. In *ICCV*, pages 10012–10022, 2021. 2
- [59] Ziwei Luo, Fredrik K Gustafsson, Zheng Zhao, Jens Sjölund, and Thomas B Schön. Controlling vision-language models for universal image restoration. *arXiv preprint arXiv:2310.01018*, 2023. 8
- [60] Ziwei Luo, Fredrik K Gustafsson, Zheng Zhao, Jens Sjölund, and Thomas B Schön. Image restoration with mean-reverting stochastic differential equations. In *ICML*, pages 23045–23066, 2023. 8

- [61] Jiaqi Ma, Tianheng Cheng, Guoli Wang, Qian Zhang, Xinggang Wang, and Lefei Zhang. Prores: Exploring degradation-aware visual prompt for universal image restoration. *arXiv preprint arXiv:2306.13653*, 2023. 8
- [62] Long Ma, Tengyu Ma, Risheng Liu, Xin Fan, and Zhongxuan Luo. Toward fast, flexible, and robust low-light image enhancement. In *CVPR*, pages 5637–5646, 2022. 7
- [63] Jiayuan Mao, Tete Xiao, Yuning Jiang, and Zhimin Cao. What can help pedestrian detection? In *CVPR*, pages 3127–3136, 2017. 2
- [64] Xintian Mao, Yiming Liu, Wei Shen, Qingli Li, and Yan Wang. Deep residual fourier transformation for single image deblurring. *arXiv preprint arXiv:2111.11745*, 2021. 5
- [65] Yiqun Mei, Yuchen Fan, Yuqian Zhou, Lichao Huang, Thomas S Huang, and Honghui Shi. Image super-resolution with cross-scale non-local attention and exhaustive self-exemplars mining. In *CVPR*, pages 5690–5699, 2020. 2
- [66] Yiqun Mei, Yuchen Fan, and Yuqian Zhou. Image super-resolution with non-local sparse attention. In *CVPR*, pages 3517–3526, 2021. 2
- [67] Seungjun Nah, Tae Hyun Kim, and Kyoung Mu Lee. Deep multi-scale convolutional neural network for dynamic scene deblurring. In *CVPR*, pages 3883–3891, 2017. 5, 6, 7, 8
- [68] Ozan Özdenizci and Robert Legenstein. Restoring vision in adverse weather conditions with patch-based denoising diffusion models. *TPAMI*, 45(8):10346–10357, 2023. 7, 8
- [69] Dongwon Park, Dong Un Kang, Jisoo Kim, and Se Young Chun. Multi-temporal recurrent neural networks for progressive non-uniform single image deblurring with incremental temporal training. In *ECCV*, pages 327–343, 2020. 5
- [70] William Peebles and Saining Xie. Scalable diffusion models with transformers. In *ICCV*, pages 4195–4205, 2023. 3
- [71] Vaishnav Potlapalli, Syed Waqas Zamir, Salman Khan, and Fahad Shahbaz Khan. Promptir: Prompting for all-in-one blind image restoration. *arXiv preprint arXiv:2306.13090*, 2023. 8
- [72] Rui Qian, Robby T Tan, Wenhan Yang, Jiajun Su, and Jiaying Liu. Attentive generative adversarial network for rain-drop removal from a single image. In *CVPR*, pages 2482–2491, 2018. 7
- [73] Xu Qin, Zhilin Wang, Yuanchao Bai, Xiaodong Xie, and Huizhu Jia. Ffa-net: Feature fusion attention network for single image dehazing. In *AAAI*, pages 11908–11915, 2020. 6
- [74] Yuwei Qiu, Kaihao Zhang, Chenxi Wang, Wenhan Luo, Hongdong Li, and Zhi Jin. Mb-taylorformer: Multi-branch efficient transformer expanded by taylor formula for image dehazing. In *ICCV*, pages 12802–12813, 2023. 6, 7
- [75] Yuhui Quan, Shijie Deng, Yixin Chen, and Hui Ji. Deep learning for seeing through window with raindrops. In *ICCV*, pages 2463–2471, 2019. 7
- [76] Yuhui Quan, Zicong Wu, and Hui Ji. Neumann network with recursive kernels for single image defocus deblurring. In *CVPR*, pages 5754–5763, 2023. 6
- [77] Yuhui Quan, Xin Yao, and Hui Ji. Single image defocus deblurring via implicit neural inverse kernels. In *ICCV*, pages 12600–12610, 2023. 6
- [78] Pejman Rasti, Tonis Uiboupin, Sergio Escalera, and Ghohamreza Anbarjafari. Convolutional neural network super resolution for face recognition in surveillance monitoring. In *Articulated Motion and Deformable Objects*, pages 175–184, 2016. 1
- [79] Jaesung Rim, Haeyun Lee, Jucheol Won, and Sunghyun Cho. Real-world blur dataset for learning and benchmarking deblurring algorithms. In *ECCV*, pages 184–201, 2020. 5
- [80] Lingyan Ruan, Bin Chen, Jizhou Li, and Miuling Lam. Learning to deblur using light field generated and real defocus images. In *CVPR*, pages 16304–16313, 2022. 6
- [81] Ziyi Shen, Wenguan Wang, Xiankai Lu, Jianbing Shen, Haibin Ling, Tingfa Xu, and Ling Shao. Human-aware motion deblurring. In *ICCV*, pages 5572–5581, 2019. 5
- [82] Zhuoran Shen, Mingyuan Zhang, Haiyu Zhao, Shuai Yi, and Hongsheng Li. Efficient attention: Attention with linear complexities. In *WACV*, pages 3531–3539, 2021. 3
- [83] Jianping Shi, Li Xu, and Jiaya Jia. Just noticeable defocus blur detection and estimation. In *CVPR*, 2015. 6
- [84] Hyeonseok Son, Junyong Lee, Sunghyun Cho, and Seungyong Lee. Single image defocus deblurring using kernel-sharing parallel atrous convolutions. In *ICCV*, pages 2642–2650, 2021. 6
- [85] Maitreya Suin, Kuldeep Purohit, and AN Rajagopalan. Spatially-attentive patch-hierarchical network for adaptive motion deblurring. In *CVPR*, pages 3606–3615, 2020. 5
- [86] Shangquan Sun, Wenqi Ren, Xinwei Gao, Rui Wang, and Xiaochun Cao. Restoring images in adverse weather conditions via histogram transformer. In *ECCV*, 2024. 1, 7
- [87] Xin Tao, Hongyun Gao, Xiaoyong Shen, Jue Wang, and Jiaya Jia. Scale-recurrent network for deep image deblurring. In *CVPR*, pages 8174–8182, 2018. 5
- [88] Fu-Jen Tsai, Yan-Tsung Peng, Yen-Yu Lin, Chung-Chi Tsai, and Chia-Wen Lin. Stripformer: Strip transformer for fast image deblurring. In *ECCV*, pages 146–162, 2022. 5
- [89] Fu-Jen Tsai, Yan-Tsung Peng, Chung-Chi Tsai, Yen-Yu Lin, and Chia-Wen Lin. Banet: a blur-aware attention network for dynamic scene deblurring. *TIP*, 31:6789–6799, 2022. 5
- [90] Zhengzhong Tu, Hossein Talebi, Han Zhang, Feng Yang, Peyman Milanfar, Alan Bovik, and Yinxiao Li. Maxim: Multi-axis mlp for image processing. In *CVPR*, pages 5769–5780, 2022. 6, 7
- [91] Jeya Maria Jose Valanarasu, Rajeev Yasarla, and Vishal M Patel. Transweather: Transformer-based restoration of images degraded by adverse weather conditions. In *CVPR*, pages 2353–2363, 2022. 7
- [92] Ashish Vaswani, Noam Shazeer, Niki Parmar, Jakob Uszkoreit, Llion Jones, Aidan N. Gomez, Lukasz Kaiser, and Illia Polosukhin. Attention is all you need. In *NeurIPS*, pages 5998–6008, 2017. 2, 3

- [93] Cong Wang, Jinshan Pan, Wei Wang, Jiangxin Dong, Mengzhu Wang, Yakun Ju, and Junyang Chen. Promptrestorer: A prompting image restoration method with degradation perception. In *NeurIPS*, pages 8898–8912, 2023. 5
- [94] Wenhao Wang, Enze Xie, Xiang Li, Deng-Ping Fan, Kaitao Song, Ding Liang, Tong Lu, Ping Luo, and Ling Shao. Pyramid vision transformer: A versatile backbone for dense prediction without convolutions. In *ICCV*, pages 568–578, 2021. 2
- [95] Xintao Wang, Ke Yu, Shixiang Wu, Jinjin Gu, Yihao Liu, Chao Dong, Chen Change Loy, Yu Qiao, and Xiaoou Tang. Esrgan: Enhanced super-resolution generative adversarial networks. *arXiv preprint arXiv:1809.00219*, 2018. 2
- [96] Xinlong Wang, Wen Wang, Yue Cao, Chunhua Shen, and Tiejun Huang. Images speak in images: A generalist painter for in-context visual learning. In *CVPR*, pages 6830–6839, 2023. 8
- [97] Yufei Wang, Renjie Wan, Wenhan Yang, Haoliang Li, Lap-Pui Chau, and Alex Kot. Low-light image enhancement with normalizing flow. In *AAAI*, pages 2604–2612, 2022. 7
- [98] Zhendong Wang, Xiaodong Cun, Jianmin Bao, Wengang Zhou, Jianzhuang Liu, and Houqiang Li. Uformer: A general u-shaped transformer for image restoration. In *CVPR*, pages 17683–17693, 2022. 1, 2, 4, 5, 6, 7
- [99] Chen Wei, Wenjing Wang, Wenhan Yang, and Jiaying Liu. Deep retinex decomposition for low-light enhancement. *arXiv preprint arXiv:1808.04560*, 2018. 7
- [100] Haiyan Wu, Yanyun Qu, Shaohui Lin, Jian Zhou, Ruizhi Qiao, Zhizhong Zhang, Yuan Xie, and Lizhuang Ma. Contrastive learning for compact single image dehazing. In *CVPR*, pages 10551–10560, 2021. 6
- [101] Wenhui Wu, Jian Weng, Pingping Zhang, Xu Wang, Wenhan Yang, and Jianmin Jiang. Uretinex-net: Retinex-based deep unfolding network for low-light image enhancement. In *CVPR*, pages 5901–5910, 2022. 7
- [102] Bin Xia, Yucheng Hang, Yapeng Tian, Wenming Yang, Qingmin Liao, and Jie Zhou. Efficient non-local contrastive attention for image super-resolution. In *AAAI*, pages 2759–2767, 2022. 2
- [103] Bin Xia, Yulun Zhang, Shiyin Wang, Yitong Wang, Xinlong Wu, Yapeng Tian, Wenming Yang, and Luc Van Gool. Diffir: Efficient diffusion model for image restoration. In *ICCV*, pages 13095–13105, 2023. 2
- [104] Jie Xiao, Xueyang Fu, Aiping Liu, Feng Wu, and Zheng-Jun Zha. Image de-raining transformer. *TPAMI*, 45(11): 12978–12995, 2023. 1, 7
- [105] Enze Xie, Junsong Chen, Junyu Chen, Han Cai, Yujun Lin, Zhekai Zhang, Muyang Li, Yao Lu, and Song Han. Sana: Efficient high-resolution image synthesis with linear diffusion transformers. *arXiv preprint arXiv:2410.10629*, 2024. 3
- [106] Li Xu, Jimmy S Ren, Ce Liu, and Jiaya Jia. Deep convolutional neural network for image deconvolution. In *NeurIPS*, 2014. 1
- [107] Xiaogang Xu, Ruixing Wang, Chi-Wing Fu, and Jiaya Jia. Snr-aware low-light image enhancement. In *CVPR*, pages 17714–17724, 2022. 7
- [108] Wenhan Yang, Shiqi Wang, Yuming Fang, Yue Wang, and Jiaying Liu. From fidelity to perceptual quality: A semi-supervised approach for low-light image enhancement. In *CVPR*, pages 3063–3072, 2020. 7
- [109] Wenhan Yang, Wenjing Wang, Haofeng Huang, Shiqi Wang, and Jiaying Liu. Sparse gradient regularized deep retinex network for robust low-light image enhancement. *TIP*, 30:2072–2086, 2021. 7
- [110] Tian Ye, Yunchen Zhang, Mingchao Jiang, Liang Chen, Yun Liu, Sixiang Chen, and Erkang Chen. Perceiving and modeling density for image dehazing. In *ECCV*, pages 130–145, 2022. 6
- [111] Tian Ye, Sixiang Chen, Jinbin Bai, Jun Shi, Chenghao Xue, Jingxia Jiang, Junjie Yin, Erkang Chen, and Yun Liu. Adverse weather removal with codebook priors. In *ICCV*, 2023. 7
- [112] Tian Ye, Sixiang Chen, Wenhao Chai, Zhaohu Xing, Jing Qin, Ge Lin, and Lei Zhu. Learning diffusion texture priors for image restoration. In *CVPR*, pages 2524–2534, 2024. 7
- [113] Syed Waqas Zamir, Aditya Arora, Salman Khan, Munawar Hayat, Fahad Shahbaz Khan, Ming-Hsuan Yang, and Ling Shao. Learning enriched features for real image restoration and enhancement. In *ECCV*, pages 492–511, 2020. 7
- [114] Syed Waqas Zamir, Aditya Arora, Salman Khan, Munawar Hayat, Fahad Shahbaz Khan, Ming-Hsuan Yang, and Ling Shao. Multi-stage progressive image restoration. In *CVPR*, pages 14821–14831, 2021. 5, 6
- [115] Syed Waqas Zamir, Aditya Arora, Salman Khan, Munawar Hayat, Fahad Shahbaz Khan, and Ming-Hsuan Yang. Restormer: Efficient transformer for high-resolution image restoration. In *CVPR*, pages 5728–5739, 2022. 1, 2, 4, 5, 6, 7, 8
- [116] Syed Waqas Zamir, Aditya Arora, Salman Khan, Munawar Hayat, Fahad Shahbaz Khan, Ming-Hsuan Yang, and Ling Shao. Learning enriched features for fast image restoration and enhancement. *TPAMI*, 45(2):1934–1948, 2022. 8
- [117] Hongguang Zhang, Yuchao Dai, Hongdong Li, and Piotr Koniusz. Deep stacked hierarchical multi-patch network for image deblurring. In *CVPR*, pages 5978–5986, 2019. 5
- [118] Jiawei Zhang, Jinshan Pan, Jimmy Ren, Yibing Song, Linchao Bao, Rynson WH Lau, and Ming-Hsuan Yang. Dynamic scene deblurring using spatially variant recurrent neural networks. In *CVPR*, pages 2521–2529, 2018. 5
- [119] Jinghao Zhang, Jie Huang, Mingde Yao, Zizheng Yang, Hu Yu, Man Zhou, and Feng Zhao. Ingredient-oriented multi-degradation learning for image restoration. In *CVPR*, pages 5825–5835, 2023. 8
- [120] Jiale Zhang, Yulun Zhang, Jinjin Gu, Yongbing Zhang, Linghe Kong, and Xin Yuan. Accurate image restoration with attention retractable transformer. In *ICLR*, 2023. 1, 3
- [121] Kai Zhang, Wangmeng Zuo, Yunjin Chen, Deyu Meng, and Lei Zhang. Beyond a gaussian denoiser: Residual learning of deep cnn for image denoising. *TIP*, 26(7):3142–3155, 2017. 1, 2
- [122] Kaihao Zhang, Wenhan Luo, Yiran Zhong, Lin Ma, Bjorn Stenger, Wei Liu, and Hongdong Li. Deblurring by realistic blurring. In *CVPR*, pages 2737–2746, 2020. 5

- [123] Xiang Zhang, Yulun Zhang, and Fisher Yu. Hit-sr: Hierarchical transformer for efficient image super-resolution. In *ECCV*, 2024. [2](#)
- [124] Yulun Zhang, Kunpeng Li, Kai Li, Lichen Wang, Bineng Zhong, and Yun Fu. Image super-resolution using very deep residual channel attention networks. In *ECCV*, pages 286–301, 2018. [2](#), [4](#)
- [125] Yulun Zhang, Yapeng Tian, Yu Kong, Bineng Zhong, and Yun Fu. Residual dense network for image super-resolution. In *CVPR*, pages 2472–2481, 2018. [2](#)
- [126] Yonghua Zhang, Jiawan Zhang, and Xiaojie Guo. Kindling the darkness: A practical low-light image enhancer. In *ACMMM*, pages 1632–1640, 2019. [7](#)
- [127] Yulun Zhang, Yapeng Tian, Yu Kong, Bineng Zhong, and Yun Fu. Residual dense network for image restoration. *TPAMI*, 43(7):2480–2495, 2021. [2](#)
- [128] Dian Zheng, Xiao-Ming Wu, Shuzhou Yang, Jian Zhang, Jian-Fang Hu, and Wei-Shi Zheng. Selective hourglass mapping for universal image restoration based on diffusion model. In *CVPR*, pages 25445–25455, 2024. [7](#), [8](#)
- [129] Shihao Zhou, Duosheng Chen, Jinshan Pan, Jinglei Shi, and Jufeng Yang. Adapt or perish: Adaptive sparse transformer with attentive feature refinement for image restoration. In *CVPR*, pages 2952–2963, 2024. [1](#), [3](#), [6](#), [7](#)
- [130] Shihao Zhou, Jinshan Pan, Jinglei Shi, Duosheng Chen, Lishen Qu, and Jufeng Yang. Seeing the unseen: A frequency prompt guided transformer for image restoration. In *ECCV*, pages 246–264, 2024. [5](#), [6](#)
- [131] Zhe Zhu, Dun Liang, Songhai Zhang, Xiaolei Huang, Baoli Li, and Shimin Hu. Traffic-sign detection and classification in the wild. In *CVPR*, pages 2110–2118, 2016. [1](#), [2](#)